Energetics of Water Expulsion from Intervening Space between Two Particles during Aggregation

Hasini S. Senanayake^a and Tuan A. Ho^{a*}
^aGeochemistry Department, Sandia National Laboratories, Albuquerque, New Mexico
87185, USA

*Corresponding author: taho@sandia.gov

Abstract

Solvent expulsion away from an intervening region between two approaching particles plays important roles in particle aggregations yet remains poorly understood. In this work, we use metadynamics molecular simulations to study the free energy landscape of removing water molecules from gibbsite and pyrophyllite slit pores representing the confined spaces between two approaching particles. For gibbsite, removing water from the intervening region is both entropically and enthalpically unfavorable. The closer the particles approach each other, the harder it is to expel water molecules. For pyrophyllite, water expulsion is spontaneous, which is different from the gibbsite system. A smaller pore makes the water removal more favorable. When water is being drained from the intervening region, single chains of water molecules are observed in gibbsite pore, while in pyrophyllite pore water cluster is usually observed. Water-gibbsite hydrogen bonds help stabilize water chains, while water forms cluster in pyrophyllite pore to maximize the number of hydrogen bonds among themselves. This work provides the first assessment into the energetics and structures of water being drained from the intervening region between two approaching particles during orientation attachment and aggregation.

1. Introduction

Oriented attachment (OA) has been identified as a non-classical crystallization pathway that generates large crystal structures by aggregating lattice-matched particles. OA was originally observed by Penn and co-workers in studies of nano-crystalline TiO₂ using atomic resolution transmission electron micrographs^{1, 2}. Thereafter, subsequent investigations have been carried out for materials that are relevant in many biological, geological, and industrial processes where structure formation cannot be explained using classical crystallization concepts³⁻⁸. OA occurs in two steps. In the first step, two particles approach each other to a proximity and remain separated by a thin layer of solvent. During this step, particles can rotate and translate to a lattice-matched configuration⁹⁻¹³. In the second step, the two particles jump into contact by eliminating the intervening solvent layer¹³. Overcoming energy barriers associated with eliminating intervening solvent layer is important for attachment to occur¹³⁻¹⁷.

The mechanism of OA, as well as its kinetics, has been studied extensively using various electron microscopic techniques^{13, 15, 18, 19}, as well as molecular simulations^{13, 14, 20-22}. These studies focused on the driving forces of OA and the effects of particle-particle, particle-solvent, and solvent-solvent interactions on OA. It has been shown that facet specific interactions facilitate the OA mechanism in several nanomaterials of variable crystal morphologies^{6, 13, 22}. Some computational studies of OA in vacuum conditions show that the electrostatic interactions between approaching particles drives OA^{23, 24}. However, many recent studies showed that intervening water can facilitate the alignment and coalescence due to water hydrogen bonding with the surfaces^{6, 11, 20, 21}. Regarding solvent expulsion during OA, in some cases, approaching particles encounter substantial energy barriers^{13, 15, 16}. In other cases, OA occurs simultaneously¹⁴.

Even though significant research progresses have been made to understand OA,

one question remains unanswered: How does expulsion of solvent from the intervening region between two approaching particles occur? This question is not only relevant to OA but also to random²⁵ and pressure-induced²⁶ aggregation. In general, it is challenging to observe experimentally the behavior and motion of intervening solvent during expulsion. Molecular simulations have been widely used to understand nanoconfined water as it can provide atomistic details of confinement and its effects. Unfortunately, to our knowledge molecular modeling has not been applied to study solvent exclusion from confined space between two approaching particles.

In this study, we apply metadynamics²⁷ molecular simulation to investigate the energetics and water structure during expulsion of water confined between two gibbsites or two pyrophyllite surfaces. The study of gibbsite aggregation is relevant to the nuclear waste management at the Hanford and Savannah River tanks. Aluminium (oxy)hydroxides are present in high concentrations in those tanks as complex aggregates²⁸, which are difficult to decompose due to unpredictable crystallization patterns²⁹. Treating nuclear waste by decomposing these complex mineral aggregates is necessary to clean up these sites. OA is one of the mechanisms that has been widely studied experimentally to understand aluminium (oxy)hydroxide aggregates³⁰⁻³². Our previous work focused on understanding gibbsite crystal face selectivity of OA¹⁷, energy barriers encountered during gibbsite particle rotating, sliding, and approaching¹¹, and role of hydrogen bonding on OA9. In this study we focus on the effect of gibbsite hydrophilicity on water expulsion. In addition, water expulsion from confined space between two pyrophyllite surfaces is also studied for comparison. Pyrophyllite is hydrophobic³³, meaning a comparison with hydrophilic gibbsite will provide an understanding of the effect of surface chemistry on water expulsion.

2. Methods

The main purpose of this work was to study the energetics of the removal of intervening water molecules from the region between two approaching particles during aggregation. We studied two systems: gibbsite-water (Figure 1a) and pyrophyllite-water (Figure 1b). In the top panel of Figure 1a, we report a simulation box containing two gibbsite layers that form a slit pore along the z direction. This slit pore represents the confining space between two approaching particles. In our previous study, we've shown that basal-basal contact is the most favorable attachment¹⁷. Therefore, in this work, the slit pores were generated using two basal (001) gibbsite surfaces. The gibbsite ribbon is periodic in the y direction and has an edge in the x direction. The method to build a gibbsite layer with edge can be found in our previous work^{9, 11, 17}. Water molecules filled the slit pore (blue region) and the green regions outside the slit pore (Figure 1a). There are always large vacuum regions along the x direction. Water molecules in the slit pore (blue region) are considered as intervening water molecules during the gibbsite particle OA. Intervening water molecules can exchange with water molecules in the solution (i.e., in green regions).

To study the energetics of water expulsion from the slit pore, we calculated the free energy or potential of mean force (PMF) as a function of number of water molecules in the blue region. The PMFs were calculated using the PLUMED package³⁴ available in LAMMPS³⁵. During the PMF calculation, the number of water molecules in the slit pore can change from zero to a pre-defined number documented later in the text. When the number of water molecules is zero, all water molecules in the slit pore move to the solution through the edges. When the number of water molecules increases from zero, water molecules move from the solution to the slit pore.

During the PMF calculation, the slit pore width does not change. To investigate the OA process (i.e., the slit pore becomes smaller and smaller), we simulated extra simulations with smaller pore size (middle and bottom panels of Figure 1a). In principle, a free energy surface with two variables (e.g., number of water molecules and pore width) is a better presentation of the aggregation process. However, obtaining such a free energy surface is practically challenging due to limited computational resources. Therefore, we calculated the PMF as a function of the number of intervening water molecules at different pore sizes ranging from 8.6 Å to 4.3 Å (e.g., number of water layers changes from 3 to 1, respectively). The pore width was determined by calculating the average z coordinate of the surface oxygen atoms. The simulation box x and y dimensions were 100.0 Å and 20.3 Å. The gibbsite particle dimension in x direction is 36.0 Å. The box z dimensions for the three pore widths are 17.0, 14.0, and 12.7 Å, respectively. There are 896 gibbsite atoms and 594, 528, and 360 water molecules for each pore width.

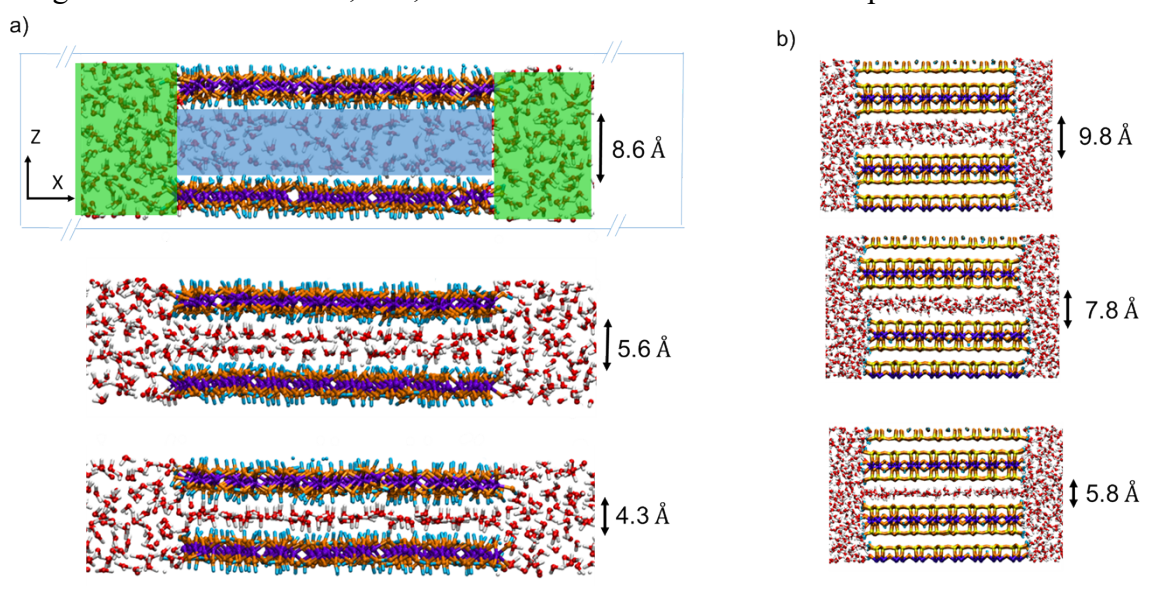


Figure 1. Simulation snapshots representing the side views of gibbsite (a) and pyrophyllite (b) pores of different pore width. Purple- Al, orange-O, cyan-H, yellow- Si, red-water O, white-water H).

The gibbsite surface is hydrophilic due to OH groups attached to octahedral Al atoms³³. To investigate how surface hydrophobicity affects water expulsion, we investigate pyrophyllite-water systems of 9.8, 7.8, and 5.8 Å pore widths (Figure 1b). To create a pyrophyllite layer with edge, we followed the method used previously to create montmorillonite with edges^{36, 37}. There are 2988 atoms for the pyrophyllite and 1664 water molecules in all pyrophyllite-water systems. The simulation box x and y dimensions are 100.0 and 31.1 Å respectively. The pyrophyllite particle dimension in x direction is 36.0 Å. The box z dimension of each pore width is 33.0, 32.0, and 31.0 Å, respectively.

Before the PMF calculation, the systems were equilibrated for 1 ns in an NVT (constant number of molecules, volume, and temperature) ensemble. All simulations were performed using a timestep of 1.0 fs. A Nosé -Hoover thermostat³⁸ with a time constant of 1 ps was used to control the temperature (300 K). A flexible SPC water model³⁹ was used to describe the water interactions. The CLAYFF force field⁴⁰ was used to describe the particle interactions with additional Al-O-H angle terms to describe edge hydroxyl groups.⁴¹ The short-range intermolecular interactions were evaluated with a cut-off distance of 10 Å, and the long-range interactions were evaluated using three-dimensional periodic boundary conditions and the particle-particle particle-mesh (PPPM) solver with a tolerance of 10^{-4} .⁴²

The well-tempered metadynamics(WTMetaD)^{27, 43, 44} simulations (i.e., PMF calculation) were carried out at 300 K in an NVT ensemble for 100 ns. The initial height of the Gaussian was set to 1.0 kcal/mol and the width was set to 1.0 Å. The Gaussians were deposited every 500 steps and the bias factor was set to 10.0. The evidence for PMF convergence was reported in the supporting information.

3. Results

In Figure 2a, we report the free energy as a function of number of water molecules in the gibbsite nanopores with different pore sizes. The free energy profiles indicate an increase in free energy with a decreasing number of water molecules in all slit pores. The gibbsite surfaces are hydrophilic due to the OH groups attached to Al atoms. Hence, the water molecules like to enter the confined environment. In other words, water expulsion from the intervening region between two gibbsite particles is an uphill process.

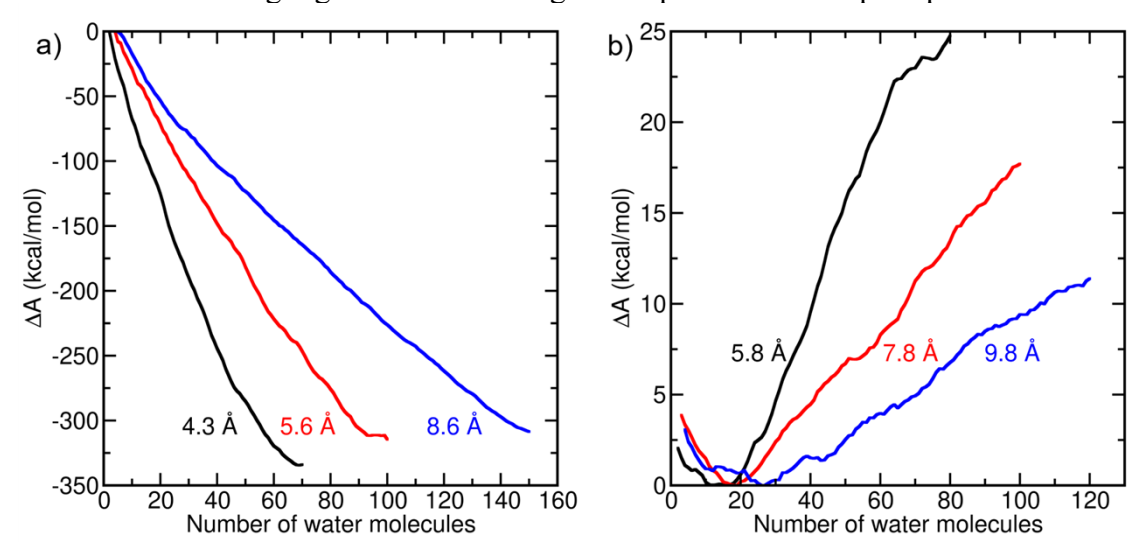


Figure 2. Free energy profiles as a function of number of water molecules in the slit gibbsite (a) and pyrophyllite (b) nanopores.

The slope of the free energy profile increases with decreasing pore width. From the largest to smallest pore width considered, the free energy necessary to remove a water molecule from the pore (i.e., negative slope of the plot) increases from 2.2 to 3.6 and 5.5 kcal/mol, respectively. Note that inside the slit pore, a water molecule experiences water/water and water-surface interactions. When the water molecules move to the solution, it only experiences water-water interactions. For comparison, we provide here a few important energy quantities related to water-water interactions, e.g., the averaged configurational energy (i.e., potential energy) is ~10 kcal/mol⁴⁵, and a water-water hydrogen bond energy is about 4.5 kcal/mol.⁴⁶ The increases in the amount of energy required to remove water from slit pore to solution when decreasing pore size suggests nanoconfinement affects water removal. The closer the particles approach each other, the harder to remove intervening water. On one hand, this will assist in maintaining a solvent separated state facilitating proper alignments and overlaps of the nanoparticles during OA. At the solvent separated state, particles can undergo different motions such as sliding and rotating until proper alignment. Effect of these motions on the OA process have been discussed elsewhere¹⁷. On the other hand, the results in Figure 2a also suggest that the final jump-into-contact step might be very difficult for gibbsite particles, unless energy is provided (e.g., drying) to eliminate the intervening water.

At the smallest pore width (4.3 Å) considered in this work, water resides within the gibbsite pore as a single water layer configuration (Figure 3a). The number of water

molecules in the slit pore is about 70. As we documented in previous work^{9, 11}, at this configuration water molecules can form two hydrogen bonds with surface hydroxyl groups and two hydrogen bonds with neighbouring water molecules. When the number of water molecules is reduced to 40 (Figure 3b), 30 (Figure 3c), or 20 (Figure 3d), isolated long and short water chains are visible. It is interesting to observe that during the water removal in the PMF calculation, water distribution in the slit pores is random and single file water configurations are regularly observed. Within a single water chain, water molecules form hydrogen bond with surfaces OH group and with neighbouring water molecules (Figure 4a).

The free energy profiles for pyrophyllite (Figure 2b) with three different pore widths suggest a completely different trend compared to the gibbsite system, i.e., water removal from the intervening region is thermodynamically favorable. The smaller the pore, the water removal is more favorable. This is expected because pyrophyllite is hydrophobic while gibbsite is hydrophilic. Reducing the pyrophyllite pore size from 9.8 to 7.8 and 5.8 Å, the slope of the energy profile increases from 0.09 to 0.17 to 0.3 kcal/mol. The magnitude of the free energy used to add or remove a water molecule from pyrophyllite slit pore is much smaller than that for gibbsite system. Note that the minimum energy for pyrophyllite in Figure 2b is observed around 20 water molecules. That is because some last water molecules form hydrogen bonds with the edge pyrophyllite, and it required some energy to remove those water molecules.

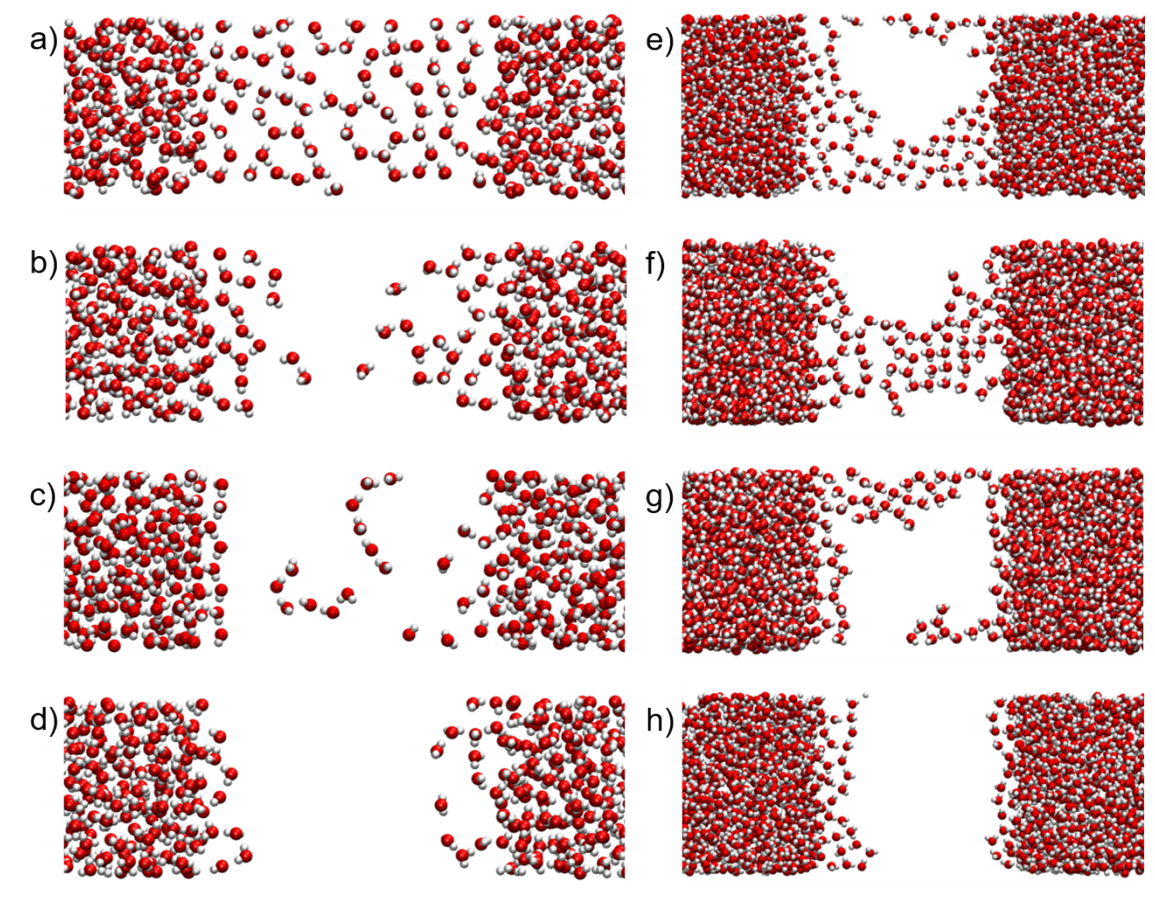


Figure 3. The simulation snapshots representing the top view (xy plane) of the water distribution in gibbsite 4.3 Å pore with 70 (a), 40 (b), 30 (c), and 20 (d) water molecules and in pyrophyllite 5.8 Å nanopore with 80 (e), 70 (f), 60 (g), and 40 (h) water molecules.

Figure 3e-h shows the snapshots during the PMF calculation for the smallest (5.8 Å) pore width of pyrophyllite. These snapshots demonstrate that during water removal, the remaining water molecules inside the slit pore form a cluster (Figure 3e-g) instead of the water chain observed for gibbsite. Water molecules in the cluster usually form hydrogen bonds with the neighbouring water molecules (Figure 4bc) and rarely form hydrogen bonds with the surface. In other words, water chain is stable in gibbsite slit pore because a water molecule can form hydrogen bond with surface. In pyrophyllite pore, because a water molecule rarely forms hydrogen bonds with surface, a cluster is the configuration in which a water molecule can maximize the number of hydrogen bonds formed with other water molecules. A more quantitative comparison of hydrogen bonding was performed for the smallest pore widths of gibbsite and pyrophyllite as shown in Figure 4d. An hydrogen bonding is determined by a geometric criteria, where R_{Od···Oa}≤ 3.6 Å, $r_{Hd\cdots Oa} \le 2.45$ Å, and $\theta_{Hd-Od\cdots Oa} \le 30^{\circ}$ (d and a denote donor and acceptor).⁴⁷ These criteria were originally defined for a water-water hydrogen bond. We applied the same criteria for water-surface hydrogen bond. This doesn't guarantee a correct definition of hydrogen bond between water-surface. Therefore, the results for water-surface hydrogen bond is for qualitatively discussion. The results in Figure 4d indicate that the number of water-water hydrogen bond in pyrophyllite pore is more than the number of water-water hydrogen bond in gibbsite pore. In addition, water-gibbsite hydrogen bond is higher than water-pyrophyllite hydrogen bond. These results support the argument about water chain and water cluster we observed from simulation snapshots (Figure 4 a,b, and c).

At smaller numbers of water molecules, such as 40 (Figure 3h), most water molecules remain close to the edge of the surface and form hydrogen bonds with the edge atoms of pyrophyllite.

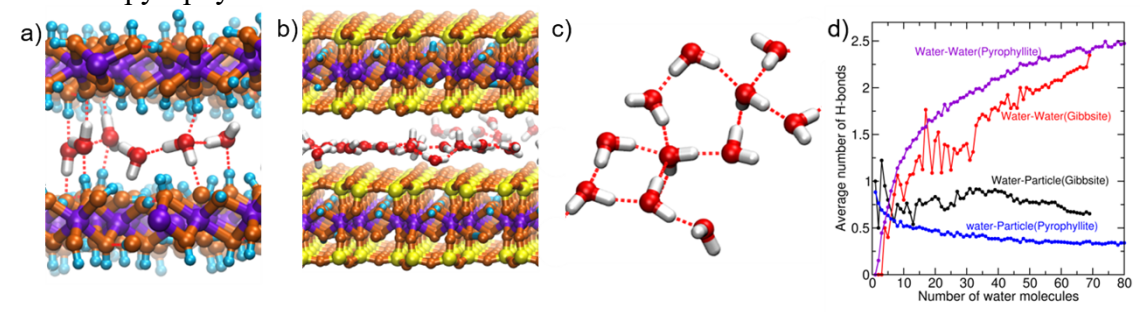


Figure 4. Side view of a water chain in gibbsite pore (a) with hydrogen bond network (red dash lines). A water in the middle of the chain can form two hydrogen bonds with the neighboring water molecules and two hydrogen bonds with the surface oxygen or hydrogen. In pyrophyllite, clusters of water are formed instead of chains (b, c). Side (b) and top (c) views illustrate the water hydrogen bond network of water cluster in pyrophyllite pore. The average number of H-bonds (d) between water-water, and water-surface as a function of number of water molecules in gibbsite 4.3 Å and pyrophyllite 5.8 Å nanopores. H-bonds were calculated only for the confined water. Water at the edges of the particle and the bulk were not considered.

We next examine the enthalpic and entropic contribution to the free energy profile obtained from fluctuation theory approach. To examine the enthalpic and entropic contribution we have applied a simple extension of fluctuation theory as proposed by Thompson and colleagues, 48 , 49 to decompose the free energy into its energetic contributions of entropy and internal energy. By assuming that the system is in equilibrium with the bias potential used in metadynamics, the Helmholtz free energy, ΔA

(x) can be calculated from the probability distribution of the collective variable (P(x)), which is in our case the number of water molecules within the pore (Equation 1).

$$\Delta A(x) = -\frac{1}{\beta} \ln \frac{P(x)}{P(x_0)} \tag{1}$$

Here, $\beta = 1/k_B T$ where k_B is the Boltzmann constant and T is the temperature (300K). $P(x_0)$ is the probability density at a reference point of x. This approach utilizes the temperature derivative of the free energy which was calculated using,

$$\frac{\partial \Delta A(x)}{\partial \beta} = \frac{\partial}{\partial \beta} \left[-\frac{1}{\beta} \ln \frac{P(x)}{P(x_0)} \right] \tag{2}$$

where P(x) was calculated by,

$$P(x) = \frac{Tr\{e^{-\beta(H+\Delta V)}e^{\beta\Delta V}\delta[x-\overline{x}]\}/Q_{\Delta V}}{Tr\{e^{-\beta(H+\Delta V)}e^{\beta\Delta V}\}/Q_{\Delta V}}$$
(3)

Here Tr indicates the trace (integration over phase space), $Q_{\Delta V}$ is the partition function and $H + \Delta V$ is the modified Hamiltonian in the presence of the bias potential.⁴⁸

This approach utilizes the temperature derivative of the free energy, hence permitting the calculation of entropy and internal energy from single temperature simulation. Decomposing the free energy into internal energy and entropy aids in understanding the driving forces of intervening water expulsion. The internal energy, ΔU , and entropy, $-T\Delta S$, contributes to the free energy for each pore width of the gibbsite systems as a function of the number of water molecules within the pore, as shown in Figure 5.

Both ΔU and $-T\Delta S$ contributions increase by decreasing the number of water molecules in the slit pore. The internal energy is the dominant contribution to the free energy. The entropy has modest effects in comparison. When removing water molecules from the pore to the solution, the internal energy increases, suggesting that gibbsite-water interactions are slightly more favorable compared to water-water interactions. The entropic contribution (- $T\Delta S$) increases, hence the entropy of the system decreases when removing water molecules from the nanopores to the solution. Therefore, a higher number of water molecules within the pore is more entropically favorable. This is because when the pore is filled with water, excess volume becomes available outside the pore which creates more disorder (note that the volume of the simulation box does not change during the PMF calculation). In other words, water expulsion from the intervening region between two gibbsites particles is entropically and enthalpically unfavorable.

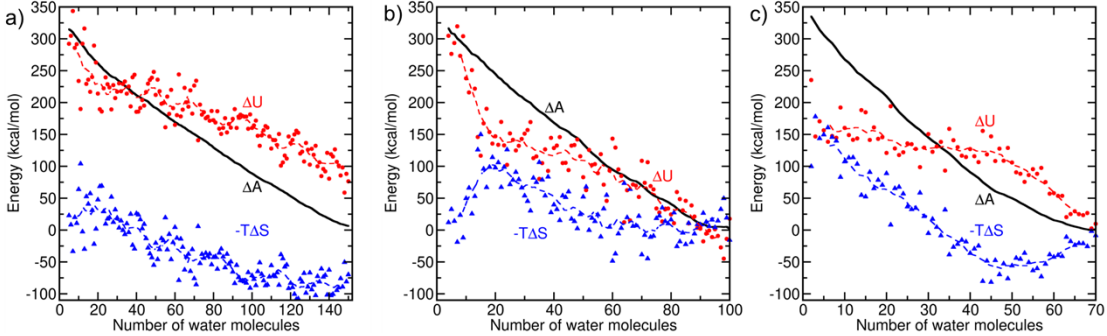


Figure 5. Internal energy (red) and entropic (blue) contributions to the free energy (black) for 8.6 (a), 5.6 (b), and 4.3 (c) Å gibbsite pores. The dashed lines show an average of every 10 data points to guide the eye.

For comparison, we also calculated the entropy using the finite difference temperature derivative of the free energy as:

$$-S = \frac{A(T + \Delta T) - U(T)}{\Delta T}$$
 (4)

Here, T=300 K and ΔT is chosen to be 30 K. The internal energy contribution, U, is calculated using, U=A+TS. The results are shown in supporting information for 4.3 Å gibbsite pore. The two calculation methods (fluctuation theory approach and finite temperature derivative) provide consistent trend for the entropic and internal energy as a function of number of water molecules in the nanopore. However, the finite temperature derivative method not only requires additional simulations, but also needs additional simulation time to produce smoother trends. Therefore, the fluctuation theory approach gives better results. We also applied the fluctuation theory approach to understand the contribution of internal energy and entropy to the free energy profile for pyrophyllite system. However, because the magnitude of the free energy change as a function of number of water molecules in pyrophyllite nanopores is very small (e.g., the scale of Figure 2b) compared to gibbsite system, a clear trend on the changes of internal energy and entropy is not visible (see supporting information). Therefore, we cannot make any conclusion about changes in internal energy and entropy as a function of water molecules in pyrophyllite nanopore.

4. Conclusion

We applied metadynamics molecular simulations to investigate the free energy of removing water molecules confined in gibbsite and pyrophyllite nanopores of three different pore widths. The interpretation of simulation results is linked to the water expulsion from the intervening region between two particles during aggregation/oriented attachment to provide an energetic picture of this poorly understanding process. For gibbsite, removing water from intervening region is energetically uphill, with unfavorable entropy and enthalpy. The closer the particles approach each other, the harder it is to expel water molecules. The results for pyrophyllite are different from that of gibbsite, i.e., water expulsion is spontaneous. The smaller the pore, the more favorable the water removal. We also observed that water can form a hydrogen bond with the gibbsite surface more abundantly resulting in long water chains in nanopore during water expulsion. For pyrophyllite system, water molecules usually form a large cluster instead of a water chain to maximize a hydrogen bond network among themselves. Overall, this work provides insight into the water expulsion from the intervening region between two particles during aggregation/oriented attachment.

Acknowledgement

This work was supported by the DOE Office of Science, Office of Basic Energy Sciences (BES), Chemical Sciences, Geosciences, and Biosciences Division. We thank Dr. Jeffery Greathouse of Sandia National Laboratories and Prof. Ward Thompson of the University of Kansas for useful discussion. This article has been authored by an employee of National Technology & Engineering Solutions of Sandia, LLC under Contract No. DE-NA0003525 with the U.S. Department of Energy (DOE). The employee owns all right, title and interest in and to the article and is solely responsible for its contents. The United States Government retains and the publisher, by accepting the article for publication, acknowledges that the United States Government retains a non-exclusive, paid-up, irrevocable, world-wide license to publish or reproduce the published form of this article

or allow others to do so, for United States Government purposes. The DOE will provide public access to these results of federally sponsored research in accordance with the DOE Public Access Plan https://www.energy.gov/downloads/doe-public-access-plan.

References

- (1) Penn, R. L.; Banfield, J. F. Oriented attachment and growth, twinning, polytypism, and formation of metastable phases; insights from nanocrystalline TiO 2. *American Mineralogist* **1998**, *83* (9-10), 1077-1082. DOI: 10.2138/am-1998-9-1016 (accessed 1/3/2024).
- (2) Penn, R. L.; Banfield, J. F. Imperfect Oriented Attachment: Dislocation Generation in Defect-Free Nanocrystals. *Science* **1998**, *281* (5379), 969-971. DOI: doi:10.1126/science.281.5379.969.
- (3) De Yoreo, J. J.; Gilbert, P. U.; Sommerdijk, N. A.; Penn, R. L.; Whitelam, S.; Joester, D.; Zhang, H.; Rimer, J. D.; Navrotsky, A.; Banfield, J. F.; et al. CRYSTAL GROWTH. Crystallization by particle attachment in synthetic, biogenic, and geologic environments. *Science* **2015**, *349* (6247), aaa6760. DOI: 10.1126/science.aaa6760 From NLM.
- (4) Politi, Y.; Arad, T.; Klein, E.; Weiner, S.; Addadi, L. Sea urchin spine calcite forms via a transient amorphous calcium carbonate phase. *Science* **2004**, *306* (5699), 1161-1164. DOI: 10.1126/science.1102289 From NLM.
- (5) Cölfen, H.; Antonietti, M. Mesocrystals: Inorganic Superstructures Made by Highly Parallel Crystallization and Controlled Alignment. *Angewandte Chemie International Edition* **2005**, *44* (35), 5576-5591. DOI: https://doi.org/10.1002/anie.200500496.
- (6) Sushko, M. L.; Rosso, K. M. The origin of facet selectivity and alignment in anatase TiO2 nanoparticles in electrolyte solutions: implications for oriented attachment in metal oxides. *Nanoscale* **2016**, *8* (47), 19714-19725, 10.1039/C6NR06953C. DOI: 10.1039/C6NR06953C.
- (7) Frandsen, C.; Legg, B. A.; Comolli, L. R.; Zhang, H.; Gilbert, B.; Johnson, E.; Banfield, J. F. Aggregation-induced growth and transformation of β-FeOOH nanorods to micron-sized α-Fe2O3 spindles. *CrystEngComm* **2014**, *16* (8), 1451-1458, 10.1039/C3CE40983J. DOI: 10.1039/C3CE40983J.
- (8) Killian, C. E.; Metzler, R. A.; Gong, Y. U. T.; Olson, I. C.; Aizenberg, J.; Politi, Y.; Wilt, F. H.; Scholl, A.; Young, A.; Doran, A.; et al. Mechanism of Calcite Co-Orientation in the Sea Urchin Tooth. *Journal of the American Chemical Society* **2009**, *131* (51), 18404-18409. DOI: 10.1021/ja907063z.
- (9) Vu, T. V.; Ho, T. A.; Criscenti, L. J. Roles of Hydrogen Bonds and Alignment in Oriented Attachment of Gibbsite Nanoparticles: Insights from Molecular Dynamics. *The Journal of Physical Chemistry C* **2023**, *127* (18), 8695-8703. DOI: 10.1021/acs.jpcc.2c08157.
- (10) Legg, B. A.; De Yoreo, J. J. Effects of Size and Shape on the Tolerances for Misalignment and Probabilities for Successful Oriented Attachment of Nanoparticles. *Langmuir* **2023**, *39* (8), 2985-2994. DOI: 10.1021/acs.langmuir.2c02789.
- (11) Ho, T. A.; Rosso, K. M.; Criscenti, L. J. Atomistic Mismatch Defines Energy—Structure Relationships during Oriented Attachment of Nanoparticles. *The Journal of Physical Chemistry Letters* **2022**, *13* (40), 9339-9347. DOI: 10.1021/acs.jpclett.2c02511. (12) Liu, L.; Legg, B. A.; Smith, W.; Anovitz, L. M.; Zhang, X.; Harper, R.; Pearce, C. I.; Rosso, K. M.; Stack, A. G.; Bleuel, M.; et al. Predicting Outcomes of Nanoparticle Attachment by Connecting Atomistic, Interfacial, Particle, and Aggregate Scales. *ACS Nano* **2023**, *17* (16), 15556-15567. DOI: 10.1021/acsnano.3c02145.

- (13) Li, D.; Nielsen, M. H.; Lee, J. R.; Frandsen, C.; Banfield, J. F.; De Yoreo, J. J. Direction-specific interactions control crystal growth by oriented attachment. *Science* **2012**, *336* (6084), 1014-1018. DOI: 10.1126/science.1219643 From NLM.
- (14) Liu, L.; Nakouzi, E.; Sushko, M. L.; Schenter, G. K.; Mundy, C. J.; Chun, J.; De Yoreo, J. J. Connecting energetics to dynamics in particle growth by oriented attachment using real-time observations. *Nature Communications* **2020**, *11* (1), 1045. DOI: 10.1038/s41467-020-14719-w.
- (15) Zhang, X.; Shen, Z.; Liu, J.; Kerisit, S. N.; Bowden, M. E.; Sushko, M. L.; De Yoreo, J. J.; Rosso, K. M. Direction-specific interaction forces underlying zinc oxide crystal growth by oriented attachment. *Nature Communications* **2017**, *8* (1), 835. DOI: 10.1038/s41467-017-00844-6.
- (16) Zhu, C.; Liang, S.; Song, E.; Zhou, Y.; Wang, W.; Shan, F.; Shi, Y.; Hao, C.; Yin, K.; Zhang, T.; et al. In-situ liquid cell transmission electron microscopy investigation on oriented attachment of gold nanoparticles. *Nature Communications* **2018**, *9* (1), 421. DOI: 10.1038/s41467-018-02925-6.
- (17) Ho, T. A.; Criscenti, L. J. Molecular-level understanding of gibbsite particle aggregation in water. *Journal of Colloid and Interface Science* **2021**, *600*. DOI: https://doi.org/10.1016/j.jcis.2021.05.016.
- (18) Zhang, X.; He, Y.; Liu, J.; Bowden, M. E.; Kovarik, L.; Mao, S. X.; Wang, C.; De Yoreo, J. J.; Rosso, K. M. Accessing crystal-crystal interaction forces with oriented nanocrystal atomic force microscopy probes. *Nat Protoc* **2018**, *13* (9), 2005-2030. DOI: 10.1038/s41596-018-0027-4 From NLM.
- (19) Wang, Y.; Peng, X.; Abelson, A.; Zhang, B.-K.; Qian, C.; Ercius, P.; Wang, L.-W.; Law, M.; Zheng, H. In situ TEM observation of neck formation during oriented attachment of PbSe nanocrystals. *Nano Research* **2019**, *12* (10), 2549-2553. DOI: 10.1007/s12274-019-2483-8.
- (20) Kerisit, S. N.; De Yoreo, J. J. Effect of Hydrophilicity and Interfacial Water Structure on Particle Attachment. *The Journal of Physical Chemistry C* **2020**, *124* (9), 5480-5488. DOI: 10.1021/acs.jpcc.9b12053.
- (21) Raju, M.; van Duin, A. C. T.; Fichthorn, K. A. Mechanisms of Oriented Attachment of TiO2 Nanocrystals in Vacuum and Humid Environments: Reactive Molecular Dynamics. *Nano Letters* **2014**, *14* (4), 1836-1842. DOI: 10.1021/nl404533k.
- (22) Sushko, M. L. Understanding the driving forces for crystal growth by oriented attachment through theory and simulations. *Journal of Materials Research* **2019**, *34* (17), 2914-2927. DOI: 10.1557/jmr.2019.151.
- (23) Spagnoli, D.; Banfield, J. F.; Parker, S. C. Free Energy Change of Aggregation of Nanoparticles. *The Journal of Physical Chemistry C* **2008**, *112* (38), 14731-14736. DOI: 10.1021/jp804966c.
- (24) Alimohammadi, M.; Fichthorn, K. A. Molecular Dynamics Simulation of the Aggregation of Titanium Dioxide Nanocrystals: Preferential Alignment. *Nano Letters* **2009**, *9* (12), 4198-4203. DOI: 10.1021/nl9024215.
- (25) Lin, M. Y.; Lindsay, H. M.; Weitz, D. A.; Ball, R. C.; Klein, R.; Meakin, P. Universality in colloid aggregation. *Nature* **1989**, *339* (6223), 360-362. DOI: 10.1038/339360a0.
- (26) Meng, L.; Vu, T. V.; Criscenti, L. J.; Ho, T. A.; Qin, Y.; Fan, H. Theoretical and Experimental Advances in High-Pressure Behaviors of Nanoparticles. *Chemical Reviews* **2023**, *123* (16), 10206-10257. DOI: 10.1021/acs.chemrev.3c00169.
- (27) Barducci, A.; Bussi, G.; Parrinello, M. Well-Tempered Metadynamics: A Smoothly Converging and Tunable Free-Energy Method. *Physical Review Letters* **2008**, *100* (2), 020603. DOI: 10.1103/PhysRevLett.100.020603.

- (28) Deutsch, W. J.; Cantrell, K. J.; Krupka, K. M.; Lindberg, M., L.; Serne, R. J. Hanford tank residual waste Contaminant source terms and release models. *Applied Geochemistry* **2011**, 26 (9-10), 1681-1693. DOI: https://doi.org/10.1016/j.apgeochem.2011.04.025.
- (29) Herting, D. L.; Cooke, G. A. *Identification of Solid Phases in Saltcake from Hanford Site Waste Tanks*; 2002. DOI: 10.2172/808264.
- (30) Liu, Y.; Ma, D.; Blackley, R. A.; Zhou, W.; Han, X.; Bao, X. Synthesis and Characterization of Gibbsite Nanostructures. *The Journal of Physical Chemistry C* **2008**, *112* (11), 4124-4128. DOI: 10.1021/jp7101572.
- (31) Freij, S. J.; Parkinson, G. M.; Reyhani, M. M. Atomic force microscopy study of the growth mechanism of gibbsite crystals. *Physical Chemistry Chemical Physics* **2004**, *6* (5), 1049-1055, 10.1039/B312505J. DOI: 10.1039/B312505J.
- (32) Anovitz, L. M.; Huestis, P.; Rampal, N.; Stack, A. G.; LaVerne, J. A.; Zhang, X.; Schenter, G. K.; Chun, J.; Legg, B. A.; Liu, L.; et al. Frustrated Coulombic and Cation Size Effects on Nanoscale Boehmite Aggregation: A Tumbler Small- and Ultra-Small-Angle Neutron Scattering Study. *The Journal of Physical Chemistry C* **2022**, *126* (9), 4391-4414. DOI: 10.1021/acs.jpcc.1c10580.
- (33) Ho, T. A.; Wang, Y. Molecular Origin of Wettability Alteration of Subsurface Porous Media upon Gas Pressure Variations. *ACS Applied Materials & Interfaces* **2021**, *13* (34), 41330-41338. DOI: 10.1021/acsami.1c11540.
- (34) Tribello, G. A.; Bonomi, M.; Branduardi, D.; Camilloni, C.; Bussi, G. PLUMED 2: New feathers for an old bird. *Computer Physics Communications* **2014**, *185* (2). DOI: https://doi.org/10.1016/j.cpc.2013.09.018.
- (35) Plimpton, S. Fast Parallel Algorithms for Short-Range Molecular Dynamics. *Journal of Computational Physics* **1995**, *117* (1), 1-19. DOI: https://doi.org/10.1006/jcph.1995.1039.
- (36) Ho, T. A.; Coker, E. N.; Jové-Colón, C. F.; Wang, Y. Control of Structural Hydrophobicity and Cation Solvation on Interlayer Water Transport during Clay Dehydration. *Nano Letters* **2022**, *22* (7), 2740-2747. DOI: 10.1021/acs.nanolett.1c04609. (37) Ho, T. A.; Coker, E. N.; Jové-Colón, C. F.; Wang, Y. Fast Advective Water Flow Through Nanochannels in Clay Interlayers: Implications for Moisture Transport in Soils and Unconventional Oil/Gas Production. *ACS Applied Nano Materials* **2020**, *3* (12), 11897-11905. DOI: 10.1021/acsanm.0c02464.
- (38) Nosé, S. A molecular dynamics method for simulations in the canonical ensemble. *Molecular Physics* **1984**, *52* (2), 255-268. DOI: 10.1080/00268978400101201.
- (39) Teleman, O.; Jönsson, B.; Engström, S. A molecular dynamics simulation of a water model with intramolecular degrees of freedom. *Molecular Physics* **1987**, *60* (1), 193-203. DOI: 10.1080/00268978700100141.
- (40) Cygan, R. T.; Liang, J.-J.; Kalinichev, A. G. Molecular Models of Hydroxide, Oxyhydroxide, and Clay Phases and the Development of a General Force Field. *The Journal of Physical Chemistry B* **2004**, *108* (4), 1255-1266. DOI: 10.1021/jp0363287.
- (41) Pouvreau, M.; Greathouse, J. A.; Cygan, R. T.; Kalinichev, A. G. Structure of Hydrated Gibbsite and Brucite Edge Surfaces: DFT Results and Further Development of the ClayFF Classical Force Field with Metal–O–H Angle Bending Terms. *The Journal of Physical Chemistry C* **2017**, *121* (27), 14757-14771. DOI: 10.1021/acs.jpcc.7b05362.
- (42) Darden, T.; York, D.; Pedersen, L. Particle mesh Ewald: An N·log(N) method for Ewald sums in large systems. *The Journal of Chemical Physics* **1993**, *98* (12), 10089-10092. DOI: 10.1063/1.464397 (accessed 1/5/2024).
- (43) Bonomi, M.; Barducci, A.; Parrinello, M. Reconstructing the equilibrium Boltzmann distribution from well-tempered metadynamics. *Journal of Computational Chemistry*

- **2009**, *30* (11), 1615-1621. DOI: https://doi.org/10.1002/jcc.21305 (accessed 2024/01/09).
- (44) Dama, J. F.; Rotskoff, G.; Parrinello, M.; Voth, G. A. Transition-Tempered Metadynamics: Robust, Convergent Metadynamics via On-the-Fly Transition Barrier Estimation. *J Chem Theory Comput* **2014**, *10* (9), 3626-3633. DOI: 10.1021/ct500441q From NLM.
- (45) van der Spoel, D.; van Maaren, P. J.; Berendsen, H. J. C. A systematic study of water models for molecular simulation: Derivation of water models optimized for use with a reaction field. *The Journal of Chemical Physics* **1998**, *108* (24), 10220-10230. DOI: 10.1063/1.476482 (accessed 1/10/2024).
- (46) Israelachvili, J. N. *Intermolecular and Surface Forces (Third Edition)*; AcademicPress:NewYork, 2011. DOI: https://doi.org/10.1016/C2009-0-21560-1.
- (47) Marti, J. Analysis of the hydrogen bonding and vibrational spectra of supercritical model water by molecular dynamics simulations. *The Journal of Chemical Physics* **1999**, *110* (14), 6876-6886. DOI: 10.1063/1.478593 (accessed 1/25/2024).
- (48) Katiyar, A.; Thompson, W. H. Temperature Dependence of Peptide Conformational Equilibria from Simulations at a Single Temperature. *The Journal of Physical Chemistry A* **2021**, *125* (11), 2374-2384. DOI: 10.1021/acs.jpca.1c00150.
- (49) Piskulich, Z. A.; Thompson, W. H. On the temperature dependence of liquid structure. *J Chem Phys* **2020**, *152* (1), 011102. DOI: 10.1063/1.5135932 From NLM.